Materials Research. 2020; 23(1): e20190676
DOI: https://doi.org/10.1590/1980-5373-MR-2019-0676

Effects of Pouring Temperature on Microstructure and Mechanical Properties of the A356 Aluminum Alloy Diecastings

***Ming Li*[a,b,*], *Yuandong Li*[c], *Hongwei Zhou*[c]**

[a]*Hexi University, Zhangye, 734000, China*
[b]*Hexi University, Zhangye, Institute of Advanced Materials Forming Technology, 734000, China*
[c]*Lanzhou University of Technology, State Key Laboratory of Advanced Processing and Recycling of Nonferrous Metals, Lanzhou 730050, China;*

Received: December 15, 2019; Revised: February 7, 2020; Accepted: March 1, 2020

Diecastings of the A356 aluminum alloy were produced by rheo-diecasting (RDC) and High pressure die casting (HPDC), the microstructures of primary solidification, secondary solidification and eutectic Si of diecastings with different pouring temperature were explored and the mechanical properties of different parameters were tested. The result shows that the primary α-Al grains in RDC with self-inoculation method (SIM) are smaller and rounder than the dendrite structure in HPDC. During the RDC process, the amount of primary α-Al grains, average grain size and the lamellar spacing of the eutectic Si increase with the decrease of the melt treatment temperature. While the average grain size and the shape factor are gradually increasing with the increase of melt treatment temperature. As a result, RDC can significantly improve the mechanical properties of the A356 aluminum alloy compared with HPDC, the mechanical properties are optimal at 600°Cwith the tensile strength and elongation are 268.67MPa and 6.8%, respectively.

Keywords: *Semisolid, Self-Inoculation Method, Primary α-Al Grain, Secondary α-Al Grain, Eutectic Si, Mechanical Property.*

1. Introduction

High pressure die casting (HPDC) is a kind of processing technology for forming metal parts, which applies high pressure to molten metal. Compared with traditional casting, HPDC are widely used in aerospace, automotive and electronic industries due to its advantages of high manufacturing accuracy, high production efficiency and low energy consumption[1,2]. Liquid metal die casting is easy to form entrainment gas in the cavity as its main filling mode is turbulence, which results in the formation of porosity defects inside the casting, and then affects the compactness of the casting structure and its mechanical properties seriously[3]. While semisolid metal die casting, which combines semisolid slurry with HPDC, can make up for the shortcomings of liquid metal die casting. As a new forming technology, the entrainment gas formed in the cavity can be effectively reduced as the main filling mode of the semisolid slurry (solid-liquid mixed state with high apparent viscosity) is laminar flow. As a result, the hole-class defects can be greatly reduced and the mechanical properties of the castings can be effectively improved[4-7].

Semisolid metal die casting includes semi-solid rheo-diecasting (RDC) and semi-solid thixotropic die casting (TDC). Compared with TDC, production costs can be significantly reduced by RDC due to short process flow and high production efficiency, hence realizes the integration of slurry preparing and forming[8]. The premise of RDC is to obtain the slurry with fine primary grains. In recent years, methods of controlling melt thermodynamic conditions[9] (such as melt overheating), inoculation treatment[10] (such as modification, suspension casting and solid-liquid mixed casting) and dynamic crystallization methods[11] (such as inclined plate casting, electromagnetic stirring) and other methods have been developed to refine the grains. And the combination of multiple technologies can make up for the limitations of a single technology in terms of grain refinement, thereby obtaining better semisolid microstructures. Based on the features of existed refinement processes such as low temperature casting, liquid-liquid mixing method, solid-liquid mixing method, suspension casting and inclined plate cooling, professor Li has developed a new method for controlling solidification microstructure, Self-Inoculation Method (SIM)[12-14]. That is, two alloys with a certain composition, quality and temperature are mixed (primary inoculation process), and then poured through a fluid director at a certain angle (secondary inoculation process) to inhibit grain growth and eliminate coarse dendrites, eventually obtain fine equiaxed crystal structures in the castings. This method is essentially a composite grain refine method derived by combining the thermodynamic grain refine method and the dynamic crystallization method.

During RDC process, the volume fraction and size distribution of primary solid phase have main effect on the mechanical properties of castings. However, not much attention has been paid on the solidification of remaining liquid in semisolid slurry. Actually, the character of remaining liquid phase also has obvious influence on the final solidification

*e-mail: 996751102@qq.com

microstructures and mechanical properties of alloys. Fan et al. studied the characteristics of the secondary solidification microstructures of Al–Si–Mg alloys using the twin-screw slurry maker process[15], and concluded that a high shear rate and shear duration combination promoted fine spherical morphology of the secondary solidification microstructures. Reisi et al.[16] believed that the stable growth of the primary particles can be maintained in the secondary solidification stage. Guan et al.[17,18] studied the solidification behavior of the remaining liquid of AZ31 alloy and AZ91 alloy, and found that the residual liquid was affected obviously by the temperature of the process. Chen et al.[19] investigated the secondary solidification behavior of AA8006 alloy, and found that the cooling rate influenced not only the primary α-Al dendrite, but also the secondary solidification process. However, the above studies did not systematically study the relationship between the solidification behavior of remaining liquid phase and mechanical properties of the final parts. Hence in present work, based on the previous researches of semisolid forming[20,21], the RDC of A356 aluminum alloy was conducted combining semisolid slurry preparation by SIM with HPDC. Microstructures of both primary solidification and secondary solidification of diecastings with different pouring temperature were analysed, the different morphology of eutectic Si caused by different pouring temperature was explored, and the mechanical properties of different parameters were tested to investigate the relationship between slurry pouring temperature, solidification behavior of remaining liquid phase and mechanical properties of the final parts.

2. Experimental Detail

The commercial A356 aluminum alloy (Chemical composition as shown in Table 1) was melted using a pit-type electric resistance furnace and degassed by C_2Cl_6 (1 mass% of alloy) over 720°C (melt temperature was measured using a K-type thermocouple), then adjusted to 700°C and directly poured into a iron mold to obtain the metal bars with the size of Φ15 mm×150 mm. Then the bars were machined into small particles with sizes of about 5 mm×5 mm×5 mm[12], which can be used as self-inoculants.

Figure 1 shows the schematic diagram of the process combining slurry preparation by SIM (self-inoculation method) with high pressure die-casting (HPDC). During the slurry preparation process, the fluid director was inclined at 45° with a length of 500 mm. The A356 alloy was melted and degassed, then adjusted the melt temperature to 690°C, 680°C and 670°C, respectively, added 5% (mass fraction of the melt) inoculants into the melt and stirred with iron bars quickly (about 5 seconds) to make them dissolved. Then the mixed melt was poured through fluid director and collected into the slurry accumulator (preheated iron crucible) to obtain semisolid slurry (the pouring temperature were adjusted and measured to be 610°C, 600°C and 590°C, respectively), and directly poured into shot chamber of DAK450-54RC die casting machine to obtain the thin-walled rheo-diecastings. As a contrast, the liquid alloy (700°C) is directly poured into shot chamber for die casting to achieve the HPDC specimens. The machine dies were preheated to 200°C and shot chamber was preheated to 400°C. Real diagram of die casting is shown in Figure 2 with the diameter of 200 mm and the wall thickness of 2 mm.

Then the diecasting parts were processed into small cubic aluminum specimens (about 10m×10mm, as shown in Figure 2). The specimens were prepared by the standard technique of grinding with SiC abrasive paper and polishing with an Al_2O_3 suspension solution, and were etched using electrolytic etching method in perchloric acid alcohol solution. Then the MFE-4 Optical microscopy was employed, and the FEG450 scanning electron microscopy was carried out equipped with an energy dispersive spectroscopy (EDS) facility and operated at an accelerating voltage of 3–20 kV to observe the solidification microstructures. The experimental solid fraction, average grain sizes ($D=(4A/\pi)^{1/2}$, where A is area of the grain) and shape factors ($F= P^2/(4\pi A)$, where P is the perimeter of grain) of primary α-Al grains and secondary α-Al grains were measured by a software of Image Proplus6.0 (take 200 grains in each group for statistical measurement, and take the average value as the final result), and the theoretical solid fraction were measured by a thermodynamics software of Pandat. The mechanical properties of diecastings were tested by WDW-100D tensile

Table 1. Chemical composition of commercial A356 alloy (*wt*%)

Si	Mg	Fe	Ti	Cu	Zn	Al
7.06	0.27	0.115	0.097	0.001	0.01	Balance

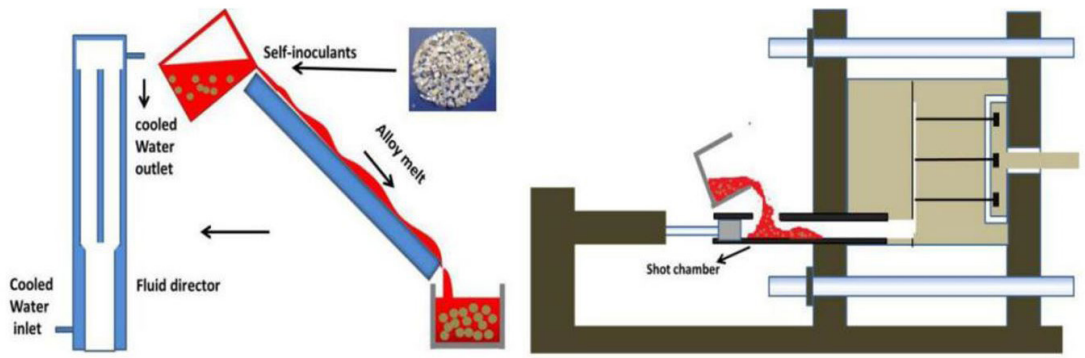

Figure 1. Schematic diagram of rheo-diecasting process by SIM.

testing machine (the specimens were machined as shown in Figure 3, and test 5 samples for each parameter, then take the average value as the final test result). Finally, the fracture morphology was analyzed by SEM.

3. Results and Discussion

3.1. Primary α-Al grains

In this experiment, the pouring temperature settings of the A356 aluminum alloy is depend on its solidification curve (as shown in Figure 4), which is plotted by theorical values that is measured using Pandat-a thermodynamic calculation software. It can be seen that the liquidus and solidus of the alloy are about 615°C and 575°C, respectively. Therefore, considering the operability of the experiment[21], the pouring temperature in RDC are 610°C, 600°C and 590°C, respectively. (it is easy to solidify completely and thus difficult to be poured if the pouring temperature is too low, such as 580°C).

Figure 2. Physical drawing and sampling position of thin-walled diecasting part.

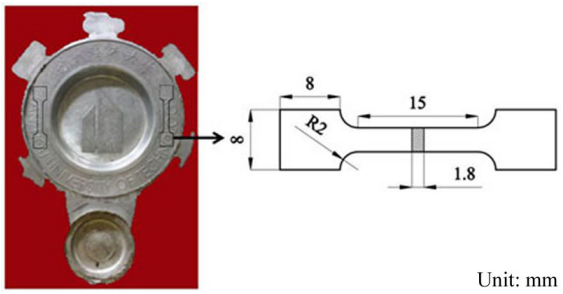

Figure 3. Sampling position and size of tensile specimens.

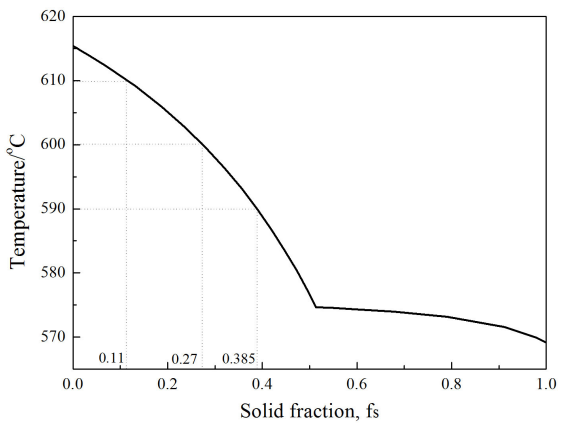

Figure 4. Solidification curve of the A356 aluminum alloy.

Figure 5 shows the microstructures of the A356 aluminum alloy with different fabricated methods. It can be seen from Figure 5 that the morphology of primary α-Al grains of the A356 aluminum alloy in liquid die-casting (700°C) is mainly dendritic. While the morphology of primary α-Al grains are non-dendritic when the pouring temperatures are between solidus and liquidus (semisolid range) of the A356 aluminum alloy (as shown in Figure 5 b,c and d). Meanwhile, the amount of primary α-Al grains are gradually increasing with the pouring temperature decreases from 610°C to 590°C.

The measured values of average grain size and shape factor of diecastings with different pouring temperature (as shown in Figure 5) are shown in Figure 6. It can be seen that both the grain size and the shape factor are the largest when the pouring temperature is 700°C. Moreover, the average grain size decreases with the increase of the pouring temperature in RDC. Both Figure 5 and Figure 6 exhibit the great effect of pouring temperature on microstructure of diecastings.

Table 2 shows the experiment values and theoretical values of solid fraction in microstructure of SIM rheo-diecasting with different pouring temperature. It can be seen that both actual solid fraction and theoretical solid fraction are gradually decreasing with the increase of pouring temperature. The solid fraction gap between the actual value and the theoretical value is mainly due to the hampering effect of the inner gate during the filling process (which was described by author's research[20]).

During the semisolid slurry preparation process by SIM, local supercooling in liquid alloy will be generated due to the temperature of the alloy melt decreased rapidly after the self-inoculants added, leading to the generation of high melting points and "large sized atomic clusters" in the local position of the melt, which can be regarded as the nucleation substrates. On the other hand, self-inoculants can be regarded as the heterogeneous nucleation substrates after adding in the melt. Moreover, the wetting angle θ of the heterogeneous nucleating substrate tends to 0° due to self-inoculant has the same composition as the base alloy, hence it greatly reduces the nucleation work and makes it easier to nucleate. Therefore, the nucleation rate increases, which is called primary inoculation process. Then the melt flows through the fluid director and the solidified shell is formed rapidly due to the chilling of director surface. After that, the dendrite fragments are formed and then involved in the melt as the subsequent melt scour and shear the solidified shell intensely, and finally evolve into rose-shape and fine dendritic primary particles, which is called secondary inoculation process. During this process, the melt temperature are decreased to the semisolid range due to the heat transfer and convection. As a result, the dendritic primary particles are survived. At the outlet of the director, turbulence occurs when two melt streams are converged, promoting thermal

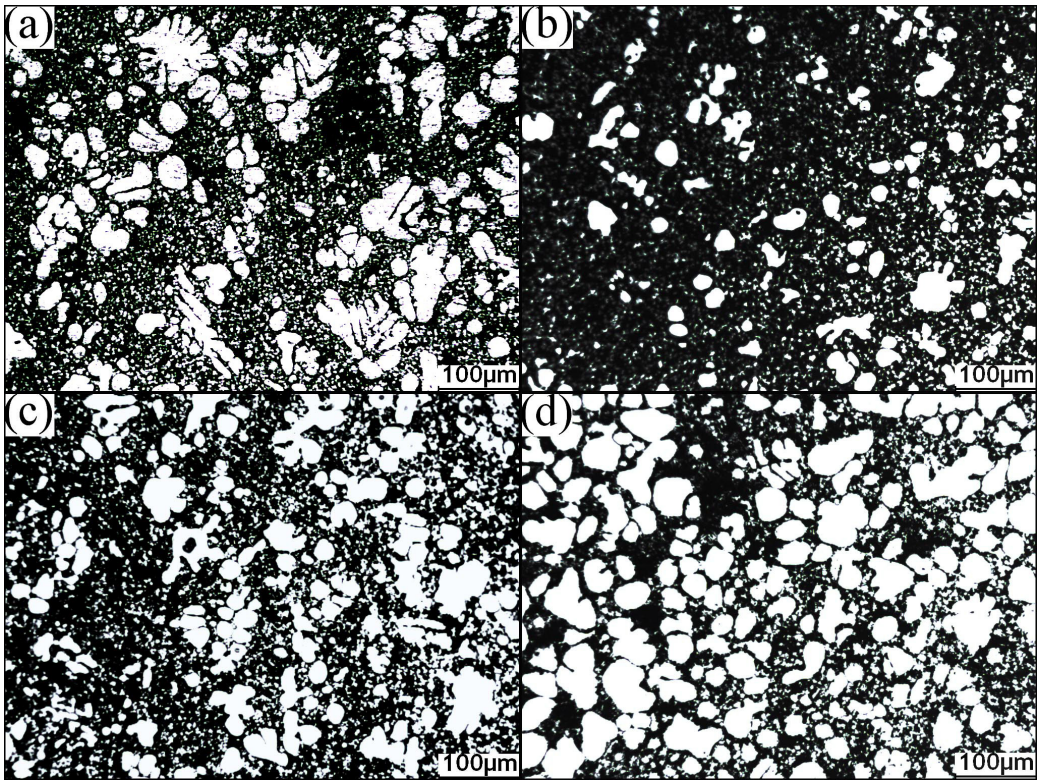

Figure 5. OM graph of the A356 aluminum alloy diecastings (a) HPDC, (b) RDC-610°C, (c) RDC-600 °C and (d) RDC-590 °C

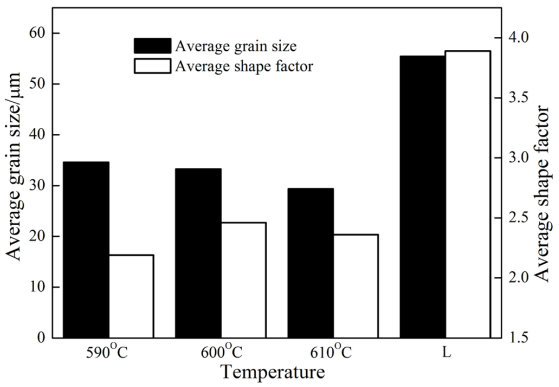

Figure 6. Measured values of average grain size and average shape factor of diecastings with different pouring temperature.

Table 2. Solid fraction of the A356 Aluminum alloy at different pouring temperature

Pouring temperature/°C	590	600	610
Actual solid fraction/%	32.9	21.6	7.1
Theoretical solid fraction/%	38.5	27.0	11.0

field and concentration field of the melt to be homogeneous. The microstructure of solidified shell at the inlet and outlet of the director have been observed and the corresponding diagram graph are plotted as shown in Figure 7. It can be seen that the microstructure of solidified shell undergoes the relatively large dendrites (at the inlet of the director), rose-like grains (at the middle of the director) and fine equiaxed grains (at the outlet of the director). Hence, after diecasting process, the microstructure exhibit the typical non-dendritic semisolid structure. The different solid fraction of the rheo-diecasting microstructure is mainly due to the different melt treatment temperature before the slurry preparation. The higher the melt treatment temperature, the higher the solid fraction of final semisolid slurry. Therefore, it can be concluded from above analysis that the semisolid slurry of the A356 aluminum alloy can be prepared by SIM. Compared with coarse dendrites in HPDC, the primary α-Al grains in RDC are uniformly distributed with fine and equiaxed morphologies.

3.2 Secondary α-Al grains

Figure 8 shows the SEM morphology of A356 aluminum alloy in different pouring temperature. It can be seen from Figure 8a that the chilled grains are fine dendrites when the pouring temperature is 700°C. While the secondary α-Al grains are fine and spherical when the pouring temperature is between 590°C and 610°C. Moreover, it can be observed by Figure 8 that the chilled grains in Figure 8a are larger than the secondary α-Al grains, while the secondary α-Al grains which are obtained from SIM rheo-diecasting are smaller and smaller with the decrease of the pouring temperature. The average grain size and shape factor of the secondary α-Al grains are measured and the results are shown in Figure 9. It can be seen that both the average grain size and the shape factor of the secondary α-Al grains are gradually increasing with the increase of pouring temperature.

Figure 10 shows the distribution rate of secondary α-Al grains of SIM rheo-diecastings with different pouring temperature. It can be seen from Figure 9a that the secondary

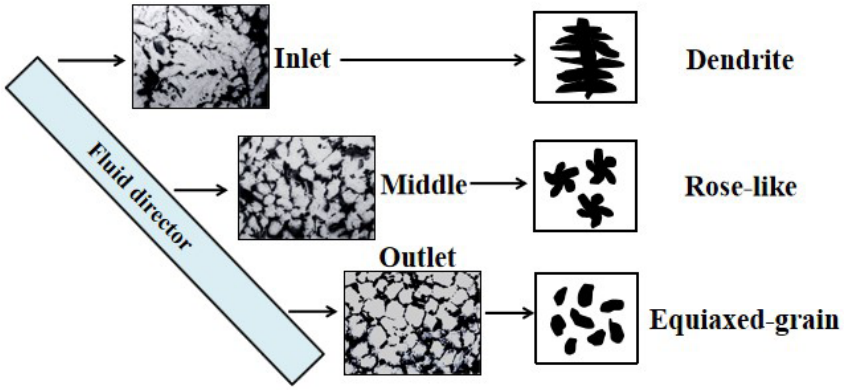

Figure 7. Microstructural evolution of A356 aluminum alloy during the secondary inoculation process.

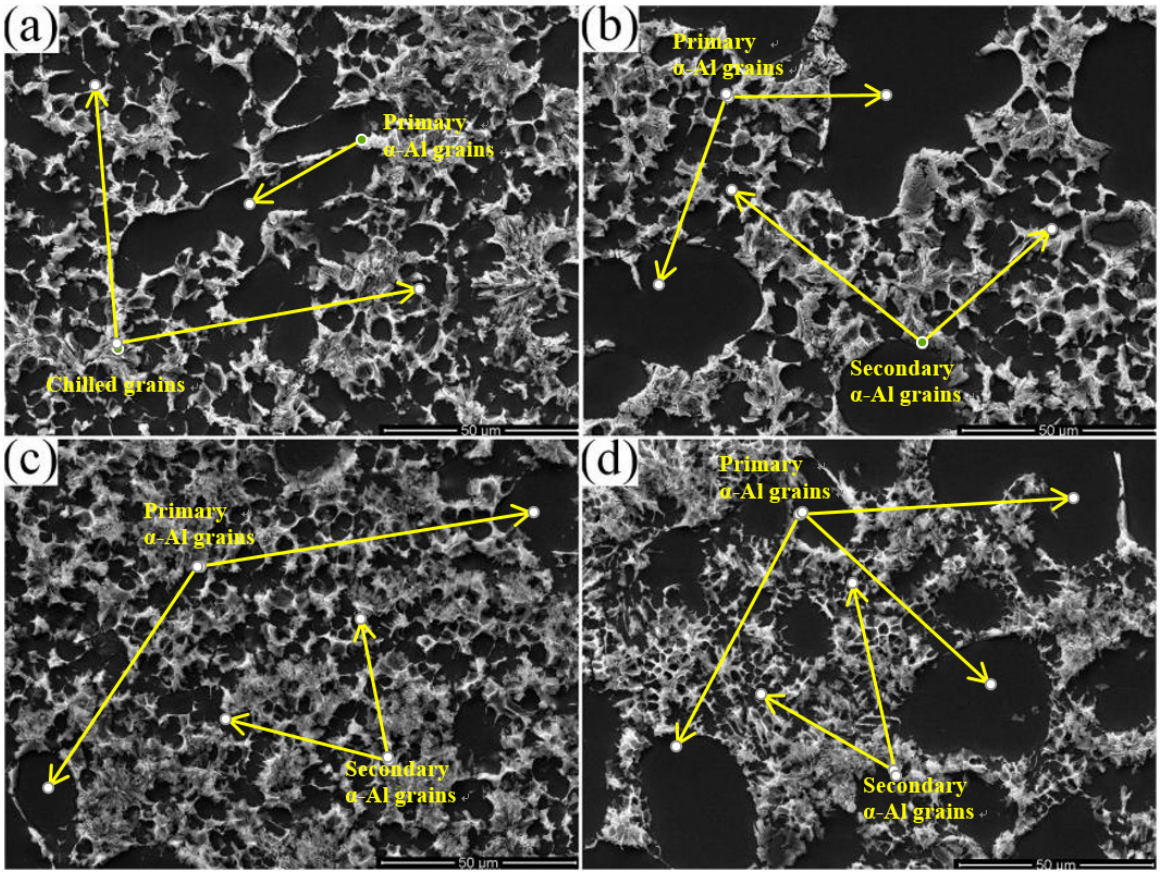

Figure 8. Solidification microstructure of diecastings (a) HPDC, (b) RDC-610°C, (c) RDC-600 °C and (d) RDC-590 °C.

α-Al grains are distributed in the range of 3μm~9μm when the pouring temperature is 590°C. While in comparison, the distribution ranges of the secondary α-Al grains are wider than 590°C when the pouring temperature are 600°C and 610°C, respectively. Furthermore, it is clearly observed that the amount of grains with the size above 9μm are gradually increasing with the increase of the pouring temperature. It can be indicated combining Figure 8, Figure 9 and Figure 10 that the pouring temperature of SIM rheo-diecasting has obviously effect on secondary solidification microstructure.

In the semisolid forming process, the secondary solidification process can be regarded as a new solidification process as primary solidification process due to it includes nucleation and growth process. According to the fundamental of solidification, the nucleation rate is increasing significantly when the value of relative supercooling is between 0.15-0.25T_m (T_m is the alloy melting temperature) for most alloy melt, which is known to be the "explosive" nucleation[22]. The T_m of the A356 aluminum alloy used in this experiment is about 615°C, while the dies are preheated to 200°C and the pouring temperature of alloy are 590°C, 600°C and 610°C,

respectively, which provide enough relative supercooling for "explosive" nucleation. Therefore, nucleating occurs throughout the whole remaining liquid in the die cavity.

In present work, the cooling rate provided by mould is hard to be measured. However, it can be rough estimated according to the Waterloo G[23], the cooling rate R satisfies the following equation:

$$R = \frac{h(T - T_0)}{c\rho z} \quad (1)$$

where h is the heat transfer coefficient, T is the pouring temperature, T_0 is the mould temperature, c is the specific heat, ρ is the density and z is the thickness of the sample. Taking c as 900J/(kg·K) and ρ as 2700kg/m^3 for aluminum alloy. In this experiment, the T_0 is 200°C and z is 2mm, and the value of h can reach 1.5×10^4Wm^{-2}K^{-1} for aluminum alloy during thin-walled die casting process[23,24]. Substituting the above values into the Equation 1, the lowest cooling rate R can reach 1200K/s. Considering the heat loss of slurry moving out of holding furnace and slurry in pressing chamber, the final cooling rate can reach 10^3K/s. Therefore, the nucleus formed by "explosive" nucleation will grow into particularly small secondary α-Al grains due to large cooling rate.

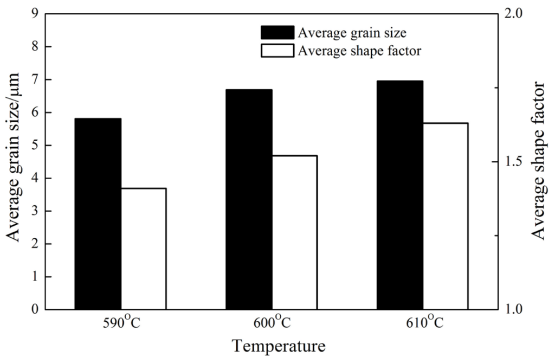

Figure 9. Measured value of average grain size and shape factor of secondary α-Al grains.

It is well known that the grain size decreases with the increase of cooling rate at the same conditions. In this experiment, all the conditions are the same except the pouring temperature. When the pouring temperature is higher, the thermal effect of the alloy liquid on the mold is greater, leading to the higher mold temperature. In addition, the higher the pouring temperature, the higher the latent heat of crystallization. As a result, the cooling rate of the alloy is reduced, and finally decreases the secondary α-Al grain size. Therefore, the secondary α-Al grain size decreases with the decrease of the pouring temperature.

Besides the difference in size and morphology, the element analysis further exhibits the distinguish between primary α-Al grains and secondary α-Al grains in RDC. Figure 11 shows the energy dispersive spectrum (EDS) analysis results in microstructure of rheo-diecasting, it can be clearly seen from line scanning that the Si content in primary α-Al grain is higher than it in secondary α-Al grain. The great difference among in primary α-Al grain, secondary α-Al grain and eutectic structure can be illustrated by point scanning values in point 1, point 2 and point 3. In primary α-Al grain, Si content is about 1.1%, which is lower than 1.6% in secondary α-Al grain. Mg, Cu, Zn are mainly existed in eutectic structure. In order to eliminate the occasionality of the experiment, content values in more points are tested as shown in Table 3, and the results prove the correctness of the above conclusions. Moreover, it is found that the Si content in primary α-Al grain increases with the distance getting closer to the grain boundary compared with the values of point 1, point 4 and point 7. In summary, it can be concluded that different solidification stages have great influence on the microstructure and composition of the alloy.

According to the phase diagram of Al-Si alloy, the maximum solubility of Si in Al is about 1.58, which is close to the Si content in secondary α-Al grains (point 2, 5 and 8 in Table 3). During the secondary solidification process of the semisolid slurry, both primary α-Al grains and secondary α-Al grains grow larger. Primary α-Al grains grow larger due to the Al atoms (precipitated in the liquid

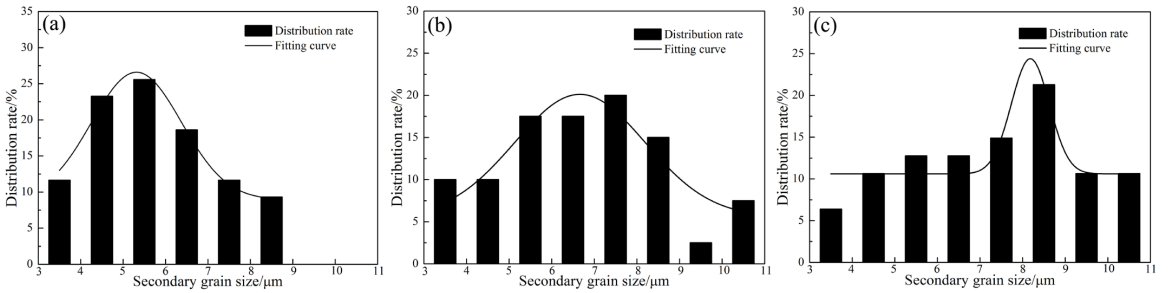

Figure 10. Distribution rate of secondary α-Al grains in RDC with different pouring temperature (a) 590 °C, (b) 600 °C and (c) 610 °C.

Table 3. Element content in each position (in Fig. 10) (*wt*.%).

Element	Point 1	Point 2	Point 3	Point 4	Point 5	Point 6	Point 7	Point 8
Al	98.9	98.4	62.3	98.8	98.3	63.4	98.5	98.4
Si	1.1	1.6	29.4	1.2	1.7	32.1	1.5	1.6
Mg	0	0	6.0	0	0	1.9	0	0
Cu	0	0	1.7	0	0	1.9	0	0
Zn	0	0	0.6	0	0	0.7	0	0

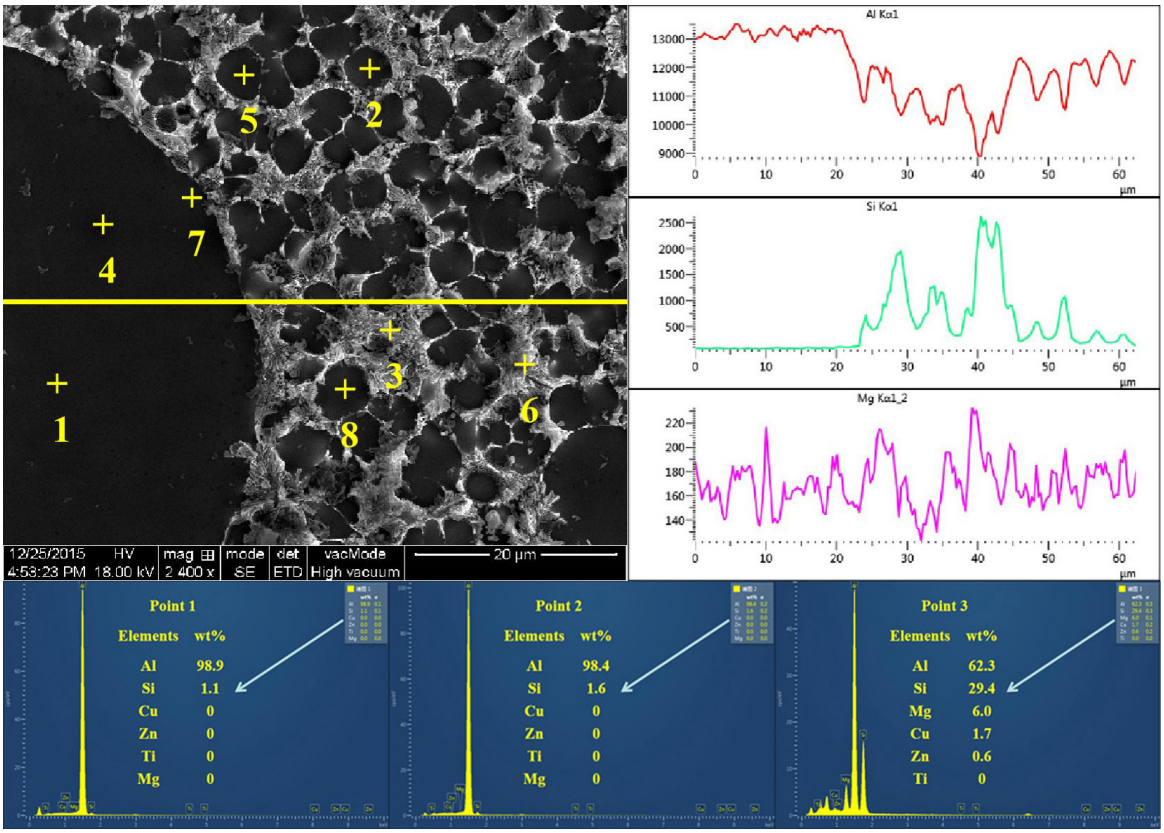

Figure 11. EDS results in microstructure of rheo-diecasting.

phase) attach to the primary α-Al grains near the primary α-Al grains[25]. Meanwhile, nucleus after "explosive" nucleation in the remaining liquid grow into secondary α-Al grains. Theoretically, the solute concentration in the remaining liquid phase is higher than that in the original alloy due to the existence of primary α-Al grains in slurry preparation process. Therefore, the content of solute in the post solidified microstructure is higher than that in the pre solidified microstructure. As a result, the solute concentration near the grain boundary is higher than center.

Figure 12 shows the elements distribution in the rheo-diecasting of the A356 aluminum alloy. Although there is a great difference in grain size between primary α-Al grains and secondary α-Al grains, the thicknesses of solute Si enriched layer in primary α-Al grains and secondary α-Al grains are the same as shown in Al and Si distribution in Figure 12. It can be indicated that the solute enrichment layer around the primary particles is formed during the secondary solidification process in the remaining liquid phase of the slurry. That is to say, the primary α-Al grains and secondary α-Al grains are growing simultaneously during the solidification of the remaining liquid phase of the slurry, which is the direct proof of the previous theoretical analysis. In addition, the growth rate of secondary α-Al grains is high due to the rapid cooling rate of die casting, leading to the Al elements precipitated in the remaining liquid phase attach to the crystallized secondary α-Al grains prior to Mg, Cu and Zn elements. As a result, Mg, Cu and Zn are enriched in the eutectic region finally.

3.3 Morphology of eutectic Si

Usually the eutectic Si is thick plate and needle like in as-cast condition, which will seriously affect the properties of the alloy. Therefore, it is necessary to obtain fine eutectic Si structure to improve the mechanical properties of the product. In general, there are two different ways to transform lamellar eutectic Si into fine fibrous Si: adding appropriate elements (chemical modification method) or accelerating cooling rate (physical method). Figure 13 shows the eutectic Si morphology of SIM rheo-diecastings with different pouring temperature. It can be seen that the pouring temperature has obvious effect on morphology of eutectic Si. When the pouring temperature is 700°C (liquid), the eutectic Si is lath and block-like. While the pouring temperature is 610°C, the eutectic Si is dendritic. As the pouring temperature further decreasing, the morphology of eutectic Si is fine fibrous (as shown in Figure 13c and d). It can be obviously shown from Figure 13 that the sizes of the eutectic Si are gradually increasing as the pouring temperature decreases from 700°C to 590°C. The eutectic Si spacing in different pouring temperature is measured as shown in Figure 14. It shows that the average lamellar spacing of the eutectic Si is gradually decreasing with the decrease of the pouring temperature.

The end of eutectic reaction marks the completion of solidification process for most alloys. The eutectic reaction in A356 aluminum alloy is L→α(Al) + β(Si), in which Al is a non-small plane phase and Si is a small plane phase. The eutectic Si is usually considered as irregular eutectic

(metal-nonmetal eutectic)[22]. According to the Jackson–Hunt theory of eutectic growth[26], the eutectic spacing λ can be expressed as follow:

$$\lambda^2 = \frac{D_L \sigma \pi^2}{m_L v \Delta S (C_\alpha - C_\beta)} \quad (2)$$

where σ is the solid-liquid interfacial tension, ΔS is the melting entropy, v is the solidification rate, m_L is the liquidus slope, D_L is the diffusion coefficient of the solute B in the liquid phase, C_α and C_β are the concentrations of solute B in α and β phases, respectively. The relationship between λ and v can be further simplified as:

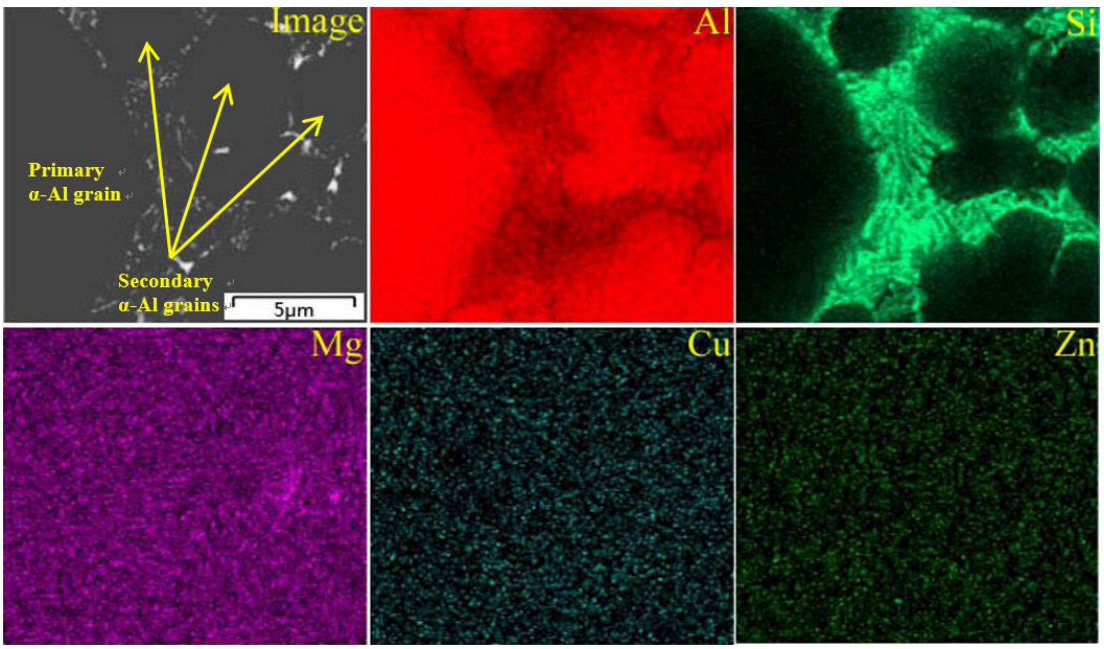

Figure 12. Elements distribution diagram of the A356 aluminum alloy in RDC.

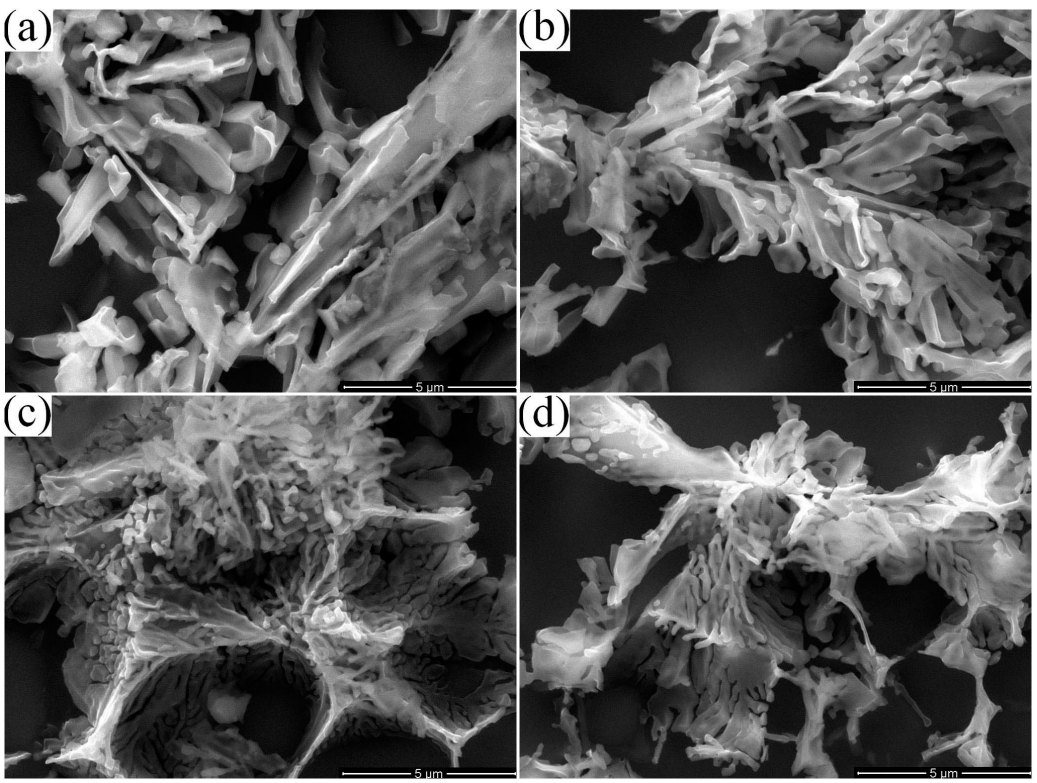

Figure 13. Eutectic Si morphology in diecastings (a) HPDC, (b) RDC-610 °C, (c) RDC-600 °C and (d) RDC-590 °C.

$$\lambda = Av^{-1/2} \tag{3}$$

here:

$$A = \sqrt{\frac{D_L \sigma \pi^2}{m_L \Delta S (C_\alpha - C_\beta)}} \tag{4}$$

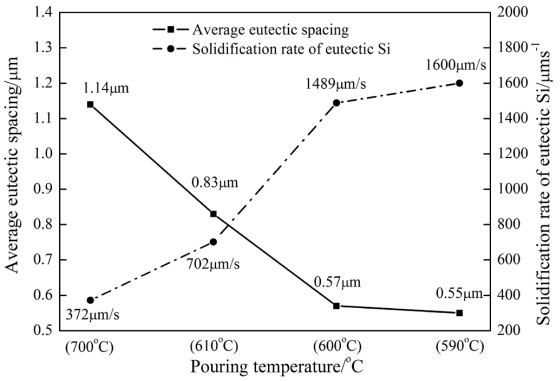

Figure 14. Average eutectic spacing and solidification rate of eutectic Si.

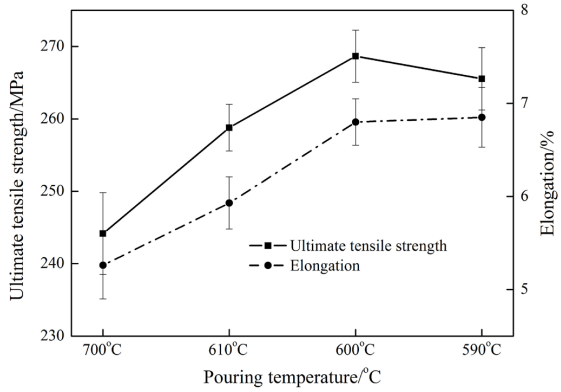

Figure 15. Mechanical properties of SIM rheo-diecastings with different pouring temperature.

which can be regarded as a constant for a specific alloy. It can be seen from the Equation 3 that the eutectic lamellar spacing λ is inversely proportional to the square root of solidification rate *v*. That is to say, the larger the solidification rate, the smaller the lamellar spacing. As for Al-Si alloy, the constant *A* was measured to be 25.2±3.2μm$^{2/3}$s$^{-1/2}$ for Al-6Si—Al-12Si alloy[27]. Substituting the eutectic spacing λ of different pouring temperature and *A* into Equation 3, the solidification rate *v* of the eutectic Si in different pouring temperature are about 372μm/s, 702μm/s, 1489μm/s and 1600μm/s, respectively, proving that the solidification rate of the eutectic Si increases with the decrease of the pouring temperature. Meanwhile, the values of the solidification rate of eutectic Si show that the RDC offers 2~4 times faster local velocity for the eutectic to grow than HPDC. More importantly, this two eutectic growth velocity are higher than 270μm/s, the measured critical velocity for the morphological change[28]. Therefore, the eutectic Si grows as fine dendrites, blocks or fibres instead of plates. In addition to the influence factor of cooling rate, there is the other reason which can not be ignored, that is: in the RDC process, the secondary α-Al grains divide the remaining liquid phase into many small intergranular regions, hence the eutectic reaction takes place in a small intergranular region, and the higher local cooling rate can promote the Si morphology transforming from dendrites to fine fibrous.

3.4 Mechanical properties

It is well known that the mechanical properties of metal materials are closely related to its microstructures. In present research, the ultimate tensile strength of rheo-diecasting specimens with different pouring temperature is tested as shown in Figure 15. It can be obtained from Figure 15 that both the ultimate tensile strength and the elongation are the lowest when the pouring temperature of the diecasting is 700°C (HPDC), with the corresponding values are 244.16MPa and 5.26%, respectively. As the pouring temperature decreasing (RDC), the ultimate tensile strength increases from 258.79MPa (when the pouring temperature is 610°C) to 268.67MPa (when the pouring temperature is 600°C) firstly, and then decreases to 265.54MPa (when the pouring

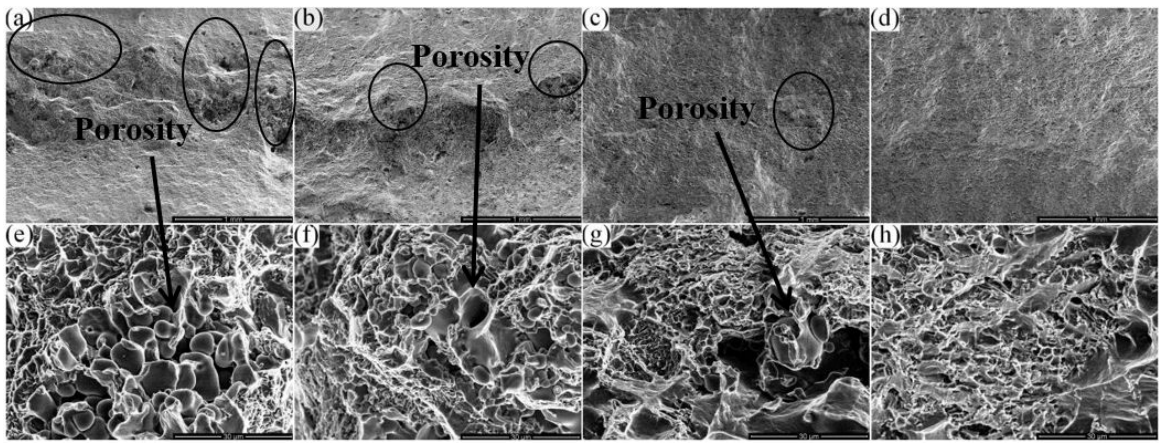

Figure 16. Fracture SEM graph of A356 aluminum alloy diecastings (a), (e) HPDC, (b), (f) RDC-610 °C, (c), (g) RDC-600 °C, (d), (h) RDC-590 °C.

Table 4. Overall average grain size of die castings at different pouring temperatures

Pouring temperature/°C	590	600	610
D/μm	24.7	14.4	10.1

temperature is 590°C). And the values of corresponding elongation are gradually increasing with the decrease of the pouring temperature (from 5.93% to 6.85%). It indicates that the pouring temperature has obvious effect on the tensile strength and elongation of the rheo-diecastings of the A356 aluminum alloy. In addition, the result clearly shows that the mechanical properties of the rheo-diecastings (semisolid diecastings produced by SIM) are higher than liquid diecastings, hence indicating that the semisolid rheo-diecasting can significantly improve the mechanical properties of A356 aluminum alloy, which can exhibit the superiority of semisolid forming process.

In order to further study the specific reasons for the differences in mechanical properties, the macro and micro fracture morphology of diecastings with different pouring temperature are employed as shown in Figure 16. It can be observed from Figure 16a that much shrinkage defects are existed in HPDC diecasting, while there are less defects in RDC diecastings. Moreover, it can be clearly seen from Figure 16b, c and d that the defect amounts are gradually decreasing with the decrease of the pouring temperature, which can further improve the the superiority of semisolid forming process. Therefore, it can be concluded that the mechanical properties of the alloy are determined by porosity, primary α-Al grains, secondary α-Al grains and eutectic structure. The air entrainment phenomenon is easy to be occurred in HPDC process due to its high pouring temperature, which is the main reason for its low mechanical properties. While in RDC process, the phenomenon of air entrainment decreases or even disappears with the increase of solid fraction due to its filling mode of laminar flow. However, the finer the grains, the better the properties of the alloy, which means that the amount of secondary α-Al grains has significant influence on mechanical property of alloy. The more the amount of secondary α-Al grains, the smaller the average grain size, the higher the mechanical properties.

The relationship between yield strength and grain size of metal alloy can be expressed by Hall-Petch formula[22]:

$$\sigma_S = \sigma_0 + Kd^{-1/2} \tag{5}$$

Where σ_s is yield strength of alloy, d is average grain diameter, σ_0 and K are material constant. It can be known that the smaller the grain size, the higher the material strength. In this experiment, the grains include primary α-Al grains and secondary α-Al grains. As the solidification curve of the A356 aluminum alloy shown (Figure 4), when the temperature of the alloy melt is 575°C, the solid fraction is reached to about 0.5 and the Al-Si eutectic reaction is started. Therefore, the overall average grain size (diameter) D can be approximately calculated as follows:

$$D = \frac{f_s d_1 + (0.5 - f_s) d_2}{0.5} \tag{6}$$

Here the d_1 and d_2 are average grain size of primary α-Al grains and secondary α-Al grains, respectively, f_s is the solid fraction of the semisolid slurry. Substituting the solid fraction values of different temperature (in Figure 4) obtain the results as shown in Table 4. It can be seen that the overall average grain size of the die casting gradually increases with the increase of pouring temperature. Hence, the mechanical properties of the die castings increase with the increase of pouring temperature in theory. However, the higher the pouring temperature, the more the remaining liquid phase. As a result, the defects in diecastings increases with the increase of pouring temperature due to the increase proportion of air entrainment, which will further decrease the mechanical properties of diecastings. Therefore, the elongation increases with the decrease of pouring temperature. In addition, the eutectic microstructure decreases with the decrease of pouring temperature, and thus increases the mechanical properties of diecastings. In summary, the mechanical property is the highest when the pouring temperature is 600°C.

4. Conclusions

1. Compared with the dendrite structure in HPDC, the primary α-Al grains of the A356 aluminum alloy in RDC with SIM are small and round. During the RDC process, both the amount of primary α-Al grains and the average grain size are gradually increasing when the pouring temperature decreases from 610°C to 590°C.
2. The secondary α-Al grains formed in RDC are smaller and rounder than chilling structure formed in HPDC. The average grain size and the shape factor increase with the increase of pouring temperature in RDC.
3. During the solidification process of the remaining liquid phase of the slurry, the primary α-Al grains and secondary α-Al grains are growing simultaneously. Si content in primary α-Al grains is higher than it in secondary α-Al grains, and Mg, Cu and Zn are enriched in the eutectic region.
4. The lamellar spacing of the eutectic Si are gradually decreasing with the decrease of the pouring temperature. In RDC, the eutectic reaction takes place in a small intergranular region due to the existence of secondary α-Al grains. Hence the higher local cooling rate can promote the Si morphology transforming from dendrites to fine fibrous.
5. The mechanical properties of the alloy are determined by porosity, primary α-Al grains, secondary α-Al grains and eutectic structure. After comprehensive consideration, the mechanical properties are optimal at 600°Cwith the tensile strength and elongation are 268.67MPa and 6.8%, respectively.

Acknowledgments

The authors would like to acknowledge the project is supported by National Natural Science Foundation of China (No. 51464031) and the Youth Foundation of Hexi University (No. QN2018011).

References

1. Zheng ZK, Yong JI, Mao WM, Yue R, Liu ZY. Influence of rheo-diecasting processing parameters on microstructure and mechanical properties of hypereutectic Al-30%Si alloy. Trans Nonferrous Met Soc China. 2017;27(6):1264-72.
2. Lumley RN, Donnell RG, Gunasegaram DR, Givord M. Heat treatment of high-pressure die castings. Metall Mater Trans, A Phys Metall Mater Sci. 2007;38(10):2564-74.
3. Chen ZW, Jahedi MZ. Die erosion and its effect on soldering formation in high pressure die casting of aluminium alloys. Mater Des. 1999;20(6):303-9.
4. Lü SL, Wu SS, Lin C, Hu ZQ, An P. Preparation and rheocasting of semisolid slurry of 5083 Al alloy with indirect ultrasonic vibration process. Mater Sci Eng A. 2011;528(29-30):8635-40.
5. Wu SS, Lü SL, An P, Nakae H. Microstructure and property of rheocasting aluminum-alloy made with indirect ultrasonic vibration process. Mater Lett. 2012;73:150-3.
6. Wang Y, Liu G, Fan Z. Microstructural evolution of rheo-diecast AZ91D magnesium alloy during heat treatment. Acta Mater. 2006;54(3):689-99.
7. Xu C, Zhao J, Guo A, Li H, Dai GZ, Zhang X. Effects of injection velocity on microstructure, porosity and mechanical properties of a rheo-diecast Al-Zn-Mg-Cu aluminum alloy. J Mater Process Technol. 2017;249:167-71.
8. Li YL, Li YD, Li C, Wu HH. Microstructure characteristics and solidification behavior of wrought aluminum alloy 2024 rheo-diecast with self-inoculation method. China Foundry. 2012;9(4):328-36.
9. Peng J, She H, Wang ZG, Pan FS. Effect of melt superheating treatment on solidification microstructure of AZ31 magnesium alloy. Trans Nonferrous Met Soc China. 2011;21(7):1497-503.
10. Liu YH, Liu XF, Li TB, Bian XF, Zhang JY. Grain refining effect of Al-Ti-C master alloy on Mg-Al alloy. Trans Nonferrous Met Soc China. 2003;13(3):622-5.
11. Li MJ, Tamura T, Miwa K. Controlling microstructures of AZ31 magnesium alloys by an electromagnetic vibration technique during solidification: from experimental obsvervation to theoretical understanding. Acta Mater. 2007;55:4635-43.
12. Li YD, Yang J, Ma Y, Qu JF, Zhang P. Effect of inoculant parameters on AM60 Mg alloy semisolid slurry prepared by self-inoculation method (II). Trans Nonferrous Met Soc China. 2010;20(11):2178-86.
13. Xing B, Hao Y, Li YD, Ma Y, Chen TJ. Microstructure control of AZ31 alloy by self-inoculation method for semisolid rheocasting. Trans Nonferrous Met Soc China. 2013;23(3):567-75.
14. Li M, Li YD, Yang WL, Zhang Y, Wang ZG. Effects of forming processes on microstructures and mechanical properties of A356 aluminum alloy prepared by self-inoculation method. Mater Res. 2019;22(3):1-11.
15. Hitchcock M, Wang Y, Fan Z. Secondary solidification behaviour of the Al-Si-Mg alloy prepared by the rheo-diecasting process. Acta Mater. 2007;55(5):1589-98.
16. Reisi M, Niroumand B. Growth of primary particles during secondary cooling of a rheocast alloy. J Alloys Compd. 2009;475(1-2):643-7.
17. Guan RG, Chen LQ, Li JP, Wang FX. Dynamical solidification behaviors and metal flow during continuous semisolid extrusion process of AZ31 alloy. J Mater Sci Technol. 2009;25(3):395-400.
18. Zhao ZY, Guan RG, Wang X, Liu CM. Microstructure formation mechanism during a novel semisolid rheo-rolling process of AZ91 magnesium alloy. Acta Metall Engl Lett. 2013;26(4):447-54.
19. Chen ZW, Zhang HF, Lei YM. Secondary solidification behaviour of AA8006 alloy prepared by suction casting. J Mater Sci Technol. 2011;27(9):769-75.
20. Li M, Li YD, Huang XF, Ma Y, Guan RG. Secondary solidification behavior of A356 Aluminum alloy prepared by the self-inoculation method. Metals (Basel). 2017;7(7):233-51.
21. Li M, Li YD, Bi GL, Huang XF, Chen TJ, Ma Y. Effects of melt treatment temperature and isothermal holding parameter on water-quenched microstructures of A356 aluminum alloy semisolid slurry. Trans Nonferrous Met Soc China. 2018;28(3):393-403.
22. Hu GX, Cai X, Rong YH. Fundamentals of Materials Science. Shangai: Shanghai Jiao Tong University Press; 2015.
23. Waterloo G, Jones H. Microstructure and thermal stability of melt-spun Al-Nd and Al-Ce alloy ribbons. J Mater Sci. 1996;31:2301-10.
24. Guo ZP, Xiong SM. Effects of alloy materials and process parameters on the heat transfer coefficient at metal/die interface in high pressure die casting. Chin Shu Hsueh Pao. 2008;44(4):433-9.
25. Li YD, Chen TJ, Ma Y, Yan FY, Hao Y. Microstructural characteristic and secondary solidification behavior of AZ91D alloy prepared by thixoforming. Trans Nonferrous Met Soc China. 2008;18(1):18-23.
26. Hunt JD, Lu SZ. Numerical modeling of cellular/dendritic array growth: spacing and structure predictions. Metall Mater Trans, A Phys Metall Mater Sci. 1996;27:611-23.
27. Grugel R, Kurz W. Growth of interdendritic eutectic in directionally solidified Al-Si alloys. Metall Mater Trans, A Phys Metall Mater Sci. 1987;18(6):1137-42.
28. Bayraktar Y, Ling D, Jones H. Formation and segregation of primary silicon in Bridgman solidified Al-18.3wt% Si alloy. Mater Sci. 1995;(30):5939-43.